Magnetoresistance effect in (La, Sr)MnO_3 bicrystalline films

J. Phys.: Condens. Matter **22** (2010) 346007 (10pp) doi:10.1088/0953-8984/22/34/346007

Magnetoresistance effect in (La, Sr)MnO_3 bicrystalline films

G Alejandro[1], L B Steren[2], H Pastoriza[1], D Vega[2], M Granada[1], J C Rojas Sánchez[1], M Sirena[1] and B Alascio[1]

[1] Centro Atómico Bariloche (CNEA), Av. Bustillo 9500, 8400 San Carlos de Bariloche, Pcia. de Río Negro, Argentina
[2] Centro Atómico Constituyentes (CNEA), 1650 San Martín, Pcia. de Buenos Aires, Argentina

E-mail: galejand@cab.cnea.gov.ar

Received 1 March 2010, in final form 7 July 2010
Published 10 August 2010
Online at stacks.iop.org/JPhysCM/22/346007

Abstract
The angular dependence of the magnetoresistance effect has been measured on bicrystalline $La_{0.75}Sr_{0.25}MnO_3$ films. The measurements have been performed on an electronically lithographed Wheatstone bridge. The study of the angular dependence of both the magnetoresistance and the resistance of single-crystalline and grain-boundary regions of the samples allowed us to isolate two contributions of low-field magnetoresistance in manganites. One of them is associated with the spin–orbit effect, i.e. the anisotropic magnetoresistance of ferromagnetic compounds, and the other one is related to spin-disorder regions at the grain boundary. Complementary x-ray diffraction, ferromagnetic resonance and low temperature magnetization experiments contribute to the characterization of the magnetic anisotropy of the samples and the general comprehension of the problem.

1. Introduction

In the last few years, the perovskite manganites have attracted renewed attention, mainly due to the huge magnetoresistance that they exhibit near the ferromagnetic (FM) ordering point [1]. The Curie temperature (T_C) signals, in these compounds, a transition from a high temperature paramagnetic (PM) insulator to a low temperature, ferromagnetic metal regime. High magnetic fields, typically of the order of several teslas, can induce the FM–PM transition above T_C. As a consequence, a huge magnetoresistance (MR) is observed around the magnetic transition, i.e. the so-called colossal magnetoresistance (CMR). In addition to CMR, it was found that these compounds also develop a low-field magnetoresistance (LFMR) very suitable for application purposes that, as shown by several studies performed on powders and polycrystalline films [2, 3], is related to the physical properties of the grain boundaries. In this context, bicrystalline substrates are especially appropriate to investigate the LFMR of manganite compounds [4], by isolating an unique artificial grain boundary (AGB). During the last few years a large amount of experimental effort has been devoted to investigate the electronic and magnetic properties of these particular systems. The LFMR of ferromagnetic perovskites, its temperature and field dependence, and the nonlinear character of the I–V curves have been studied on (La, Ca)MnO_3 [4–9], (La, Sr)MnO_3 [6, 10–12] and Sr_2FeMoO_6 [13] bicrystalline films by using different lithographed patterns of diverse size, shape and complexity. The microstructural properties have been investigated by local techniques such as x-ray microdiffraction [14] and atomic and magnetic force microscopies [15, 16], adding experimental evidence that demonstrates that film thickness, strain distribution and magnetic domain structure are closely related to the LFMR of bicrystalline manganite films. A very recent paper [17] reports on the domain wall depinning and magnetoresistance in $La_{0.7}Sr_{0.3}MnO_3$ thin films. In these systems, nanoconstrictions were created intentionally by focused-ion-beam milling.

Different theoretical approaches have been used to explain the nature of the LFMR in these systems: a Jullière-like model to explain the 'two-level ideal switch' character of the LFMR when the magnetic field is parallel to the AGB [7], spin-polarized transport with 'band bending' at the AGB [18] and the existence of a disordered narrow paramagnetic grain-boundary layer [9] have been claimed to explain the features of LFMR in manganite bicrystalline films. García *et al* [19] have proposed a two-crystal model that estimates the

pinning of domain walls to the grain boundary between them and the tunnelling across the AGB in terms of the angle between the crystal orientation of the grains. It shows that the orientation of the applied magnetic field (**H**) relative to the anisotropy axes at both sides of the AGB determines the tunnelling process between the two domains, thus governing the LFMR. Later, further work based on a similar Stoner–Wolfhart model [20] incorporating biaxial anisotropy [21] explored the magnetization reversal process for the magnetic field oriented parallel and perpendicular to the AGB.

The purpose of this work is to contribute to the comprehension of the subtle mechanisms underlying the LFMR of ferromagnetic manganites. To pursue this goal we have chosen the approach of exploring the relation between the magnetic anisotropy of the films and the angular behaviour of the LFMR. Therefore, we have performed very careful transport measurements as a function of the orientation of the samples on an (La, Sr)MnO_3 bicrystal. These were complemented with ferromagnetic resonance (FMR) and low temperature magnetization experiments carried out to identify and quantify the different anisotropy terms (magnetocrystalline, shape, substrate-induced, etc).

Our resistance versus field (R versus H) curves are strongly angle-dependent. They are also hysteretic for all the measured angular orientations, as are the others reported in the literature [4, 10, 11, 13, 20]. The shape of all our curves is smooth, in contrast to some other previous results [6, 10, 11], where a very abrupt, switch behaviour was observed. Surprisingly, it is very clear for certain orientations of our bicrystals that there are two pairs of peaks instead of the unique pair of maxima found in previous references [4, 6, 10–13, 20].

The shape of resistance versus angle curves (at fixed H) suggests that there are multiple mechanisms contributing to the MR at low field and temperature. We have identified first the CMR component that is intrinsic to FM manganites, while the LFMR itself presents two contributions. The first one correlates well with the magnetocrystalline anisotropy, as it presents similar angle dependence to the magnetization hysteresis loops. Therefore, it should not be strictly associated with the AGB, and could be attributed to the re-orientation of magnetic domains. The second contribution is indeed purely ascribed to the presence of the AGB as it exhibits the same uniaxial symmetry along the junction. Our experimental results demonstrate that, while the first (magnetocrystalline) component of the LFMR tends to vanish at the higher magnetic fields explored, the AGB component remains almost constant.

2. Samples and experimental set-up

$La_{0.75}Sr_{0.25}MnO_3$ films of 1200 Å thickness were deposited by dc sputtering on 0.5 × 0.5 cm bicrystalline $SrTiO_3$ substrates, at a temperature of 760 °C. The films are ferromagnetic below $T_C = 300$ K with a saturation magnetization of $M_S(T = 5\ \text{K}) = 530$ emu cm^{-3}. The films undergo a metal–insulator transition at $T_{MI} = 265$ K. The critical temperatures and magnetic parameters are comparable to values reported in the literature for similar (La, Sr)MnO_3 compounds [22].

X-ray diffraction measurements were performed in order to orient the samples using a four-circle diffractometer.

Ferromagnetic resonance spectra were measured at $T = 125$ K in a Bruker ESP300 spectrometer, at a working frequency of 9.5 GHz (X band). The sample was rotated around an axis normal to the plane of the film. The static magnetic field (**H**) remained always parallel to this plane during the whole experiment. DC magnetization was measured at 85 K in a vibrating sample magnetometer (VSM) using the same geometry.

The transport measurements were done by using the standard four-contact method. In order to measure the resistivity of the artificial grain boundary (AGB), Wheatstone bridges of micrometric track widths were defined by electron lithography and patterned by argon ion milling. They were designed in such a way that two arms of the bridge crossed the AGB several times (type I, or AGB arms) and the other two did not (type II, or SC arms). The SEM micrograph in figure 1 shows the dimensions and details of the lithography and the right panel schematizes the electronic circuit. The current (typically 1 μA) was injected across the pattern and, due to the geometry of the bridge, the experimental voltage V_{GB} gives a direct measure of the resistivity of the AGB [4, 11]. More precisely

$$V_{GB} = \frac{R_{GB}}{2} I. \tag{1}$$

This equivalence implicitly assumes an ideal situation where the four resistances R_{SC} (see figure 1) that constitute the single-crystal contributions to the total resistance are identical. Under this hypothesis, their corresponding voltages cancel out when measuring V_{GB}, leaving only the pure AGB contribution to the resistance. By selecting the current and voltage contacts properly, we can also measure the single-crystal contribution (V_{SC}) coming from one-half of the film, without crossing the AGB. Therefore, resistivity measurements from both the AGB region and from the single-crystalline film have been obtained. In both cases, the angular variation of the signal was collected by recording the resistivity for different angles between the AGB and the magnetic field (**H**). We kept fixed the direction of (**H**) always parallel to the plane of the films and allowed the sample to rotate. In this way we obtained a set of magnetoresistance curves at 77 K for different values of the angle between H and the AGB.

3. Structural characterization

3.1. Orientation of the $SrTiO_3$ bicrystalline substrates

The $SrTiO_3$ substrates employed in this work are commercial bicrystals with a nominal 24° misorientation angle between crystalline axes at both sides of the AGB. In order to accurately specify the meaning of this statement, we performed careful x-ray diffraction measurements on the substrates. The characterization procedure of a clean $SrTiO_3$ substrate was done in a four-circle diffractometer, especially adequate for single-crystalline samples. We probed the substrate in three different regions: at each side, far from the AGB, and on the junction itself. On one side we identified the

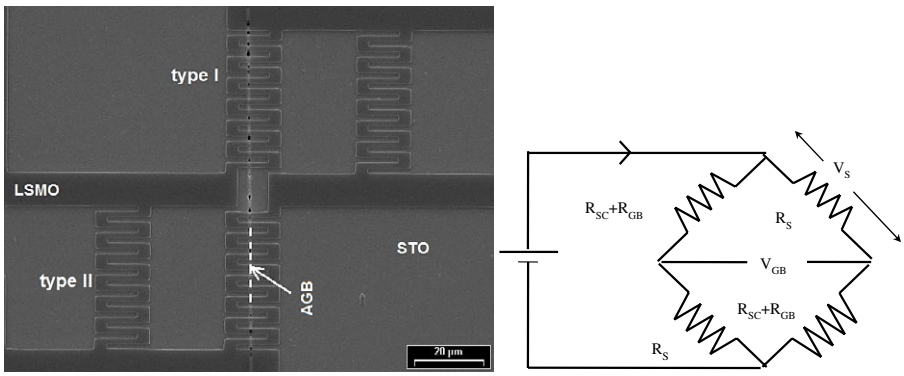

Figure 1. SEM image of the Wheatstone bridge lithographed from an $La_{0.75}Sr_{0.25}MnO_3$ (LSMO) bicrystalline film (dark grey zig-zag path). The light grey background is the STO substrate. The position of the AGB is indicated by a dashed line; the type of arms (I and II) and the different voltages and resistances are also indicated. Bar = 20 μm. Right panel: electrical circuit representing the bridge.

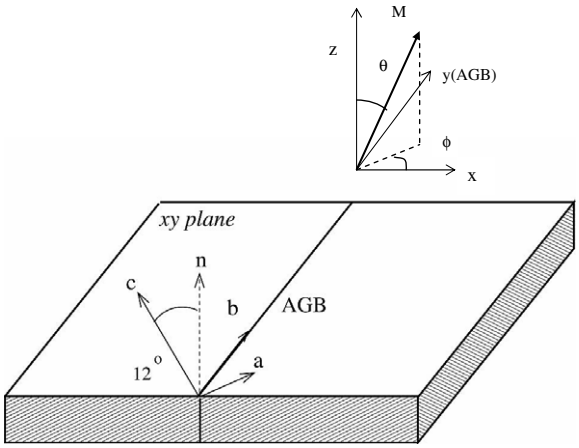

Figure 2. Orientation of laboratory frame (x, y, z) and crystalline axes (a, b, c) corresponding to the left half of the bicrystalline substrate (n indicates the normal to the xy plane).

reflections (0, 0, 1), (0, 0, 2), (1, 0, 1), (0, −1, 1), (0, −1, 2), (1, 1, 2) and (1, −1, 2) of the substrate; while on the other far side the observed reflections were (0, 0, 1), (0, 1, 1), (−1, 0, 1), (−1, 1, 1), (−1, −1, 1), (−2, 0, 1), (−2, 1, 1) and (−2, −1, 1). As expected, when measuring on the AGB region we could clearly observe reflections coming from both halves of the film. The analysis of the observed reflections revealed that the orientation of the cubic axes of the $SrTiO_3$ substrates is the one shown in figure 2.

The AGB direction is parallel to the b axis, which is common to both halves of the substrate. Each of the c axes are not perpendicular to the plane and form angles of approximately ±12° with the film normal. As deduced from the spatial position of the (0 0 1) reflections, the c axes determine a misorientation angle of 25.3°. In previous reports [4, 10, 11, 13, 20], the nominal misorientation angle of the bicrystals (12°, 24°, 36°, etc) was always contained *in the plane of the substrate*. It is important to note that, in our case, instead, this angle is confined to the plane *perpendicular* to the AGB, configuring a different geometry. The laboratory coordinate frame that we will use to describe our experiments is shown in the inset of figure 2: the xy plane coincides with the substrate plane and the y axis has been chosen coinciding with the AGB. The polar (θ) and azimuthal (ϕ) angles orient the magnetization vector **M** in this coordinate frame. In what follows, the azimuthal angle ϕ_H (not shown in figure 2) is measured from the x axis to the magnetic field vector, **H**.

3.2. Structure and epitaxy of films and substrates

Once we have deduced that the normals to the (001) planes at each site of the AGB are 12° off the substrate normal, we performed conventional θ–2θ scans in a powder diffractometer to explore the epitaxy of the (La, Sr)MnO_3 (LSMO) films. For this purpose it was necessary to modify the usual set-up employed to collect powder diffractograms. We adapted the experiment by introducing an offset of 12° to the θ angle of the detector. With this procedure we ensure that the (00k) planes (k an integer number) of the STO substrate are set into the Bragg condition. The spectrum was collected for 2θ ranging from 22° to 78° with a resolution of 0.02°, using Cu Kα radiation. Figure 3 shows a diffractogram obtained with this set-up, illuminating only one-half of the bicrystal. By doing this we can be sure that we are not collecting reflections from both sides of the substrate into the same diffractogram.

All the peaks can be identified exclusively as (00k) reflections of the substrate and the manganite film. No other types of reflections are observed. This confirms that the film grows textured along the c direction of the substrate. The inset in figure 3 shows a shorter θ–2θ scan where both the (002) reflections of film and substrate are displayed in more detail. Note that the splitting of the substrate peak is due to the natural splitting of the incident Cu Kα radiation. From the 2θ value of the (002) peaks we have deduced that the c lattice constants are 3.905 Å and 3.853 Å for the cubic STO substrate and the pseudo-cubic (La, Sr)MnO_3 film, respectively. We find that the value of the c lattice constant of the films represents a contraction of 0.4% with respect to bulk LSMO samples of similar composition. The measured values are in good agreement with previously reported cell parameters of $SrTiO_3$ and LSMO films [23, 24]. We have also collected rocking curves of the bicrystalline STO substrates from several different Bragg reflections, and from (00k) reflections of the

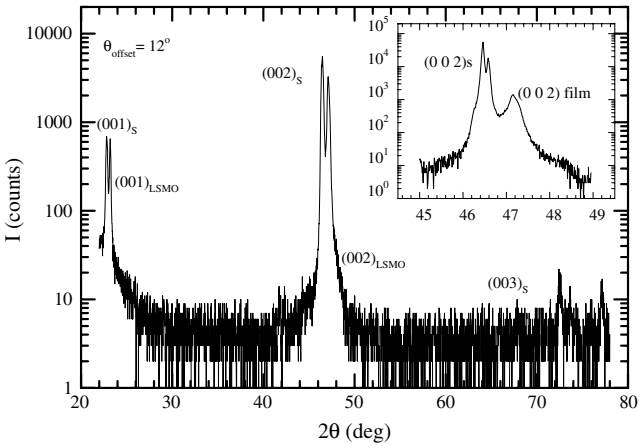

Figure 3. Room temperature diffractogram showing the $(00k)$ reflections of the $SrTiO_3$ substrate (denoted by S) and the manganite film (denoted by LSMO). Inset: detailed spectrum of the (002) peaks (step = 0.01°).

bicrystalline film. For a few specific reflections, the rocking curves of the substrate show some distortion in the peak shape. Though the films are seen to grow well textured along the *c* direction of the substrate, this observation suggests that probably small crystalline misorientations exist that could induce some degree of misorientation in the films.

4. Magnetic characterization

4.1. Low temperature magnetization

The low temperature magnetization of the non-patterned (La, Sr)MnO_3 bicrystalline films was studied as a function of the orientation of **H** relative to the AGB. To this purpose, a sequence of hysteresis loops was performed in the ferromagnetic phase at $T = 85$ K by rotating the sample around an axis perpendicular to the film, and keeping **H** in the plane of the film. A selection of these loops is shown in figure 4, where by M we actually mean the projection of the total magnetization vector **M** along the direction of **H**. The data of coercive field (H_c) and remnant magnetization (M_{rem}) values were extracted from these loops and plotted in figure 4 (bottom) as a function of the azimuthal angle ϕ_H.

A clear dependence of both parameters on the orientation of the sample is observed. The local minima ('hard' magnetization directions) are $\phi_H = 0°, 90°$ while $\phi_H \simeq 60°$ is a local maximum ('easy' magnetization direction). The difference of the values of H_c and M_{rem} at the AGB direction ($\phi_H = 90°$) and its perpendicular ($\phi_H = 0°$) is understood by assuming the existence of an uniaxial anisotropy along the AGB, superimposed on a fourfold anisotropy associated with the pseudo-cubic structure of the LaSrMnO compound. It is well known that substrate-induced stresses and morphologies give rise to additional anisotropy terms of different symmetries in manganite films [25–27]. Therefore, we attribute the uniaxial anisotropy term to film strains [27]. The deviation of the easy axes from the expected ±45°, which are found in pseudo-cubic (La, Sr)MnO_3 films [21], is also explained by

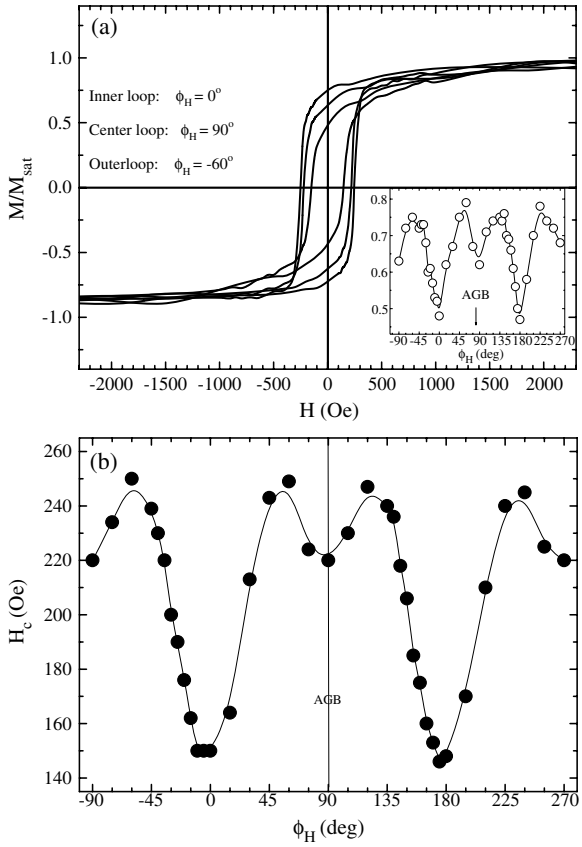

Figure 4. (a) Some hysteresis loops for particular orientations of the bicrystal. Inset: normalized remnant magnetization (M_{rem}/M_{sat}) versus ϕ_H. (b) Angular variation of the coercive field, H_c. The lines are guides to the eye. $T = 85$ K.

the presence of this uniaxial anisotropy, which bends the easy direction closer to the $\phi_H = 90°$ direction. These conclusions are in good qualitative agreement with the FMR experiments, as we will see below.

4.2. Ferromagnetic resonance

We have studied in detail the FMR spectra at $T = 125$ K, well below the ferromagnetic–paramagnetic transition (which occurs close to room temperature), as the experimental conditions such as the coupling of the radio frequency cavity and the quality of the resonance signal are simultaneously satisfactory at this temperature. Let ϕ_H be the angle between the x axis and the static magnetic field, **H**. The left panel of figure 5 shows some selected FMR spectra for different values of ϕ_H.

The main feature of each spectrum is a broad, essentially single, FMR line. This is consistent with previous electron paramagnetic resonance (EPR) results on polycrystalline [28] and single-crystalline manganites [29]. A subtle superstructure that cannot be resolved may be originated from minor crystalline misorientations coexisting in the manganite films, as discussed at the end of the section 3. As seen in the figure, H_{res} varies with the orientation of the sample. It is maximum for $\phi_H = 0°$ and minimum for $\phi_H = 45°$. These mean that the {110} directions of the cubic substrate are easy axes

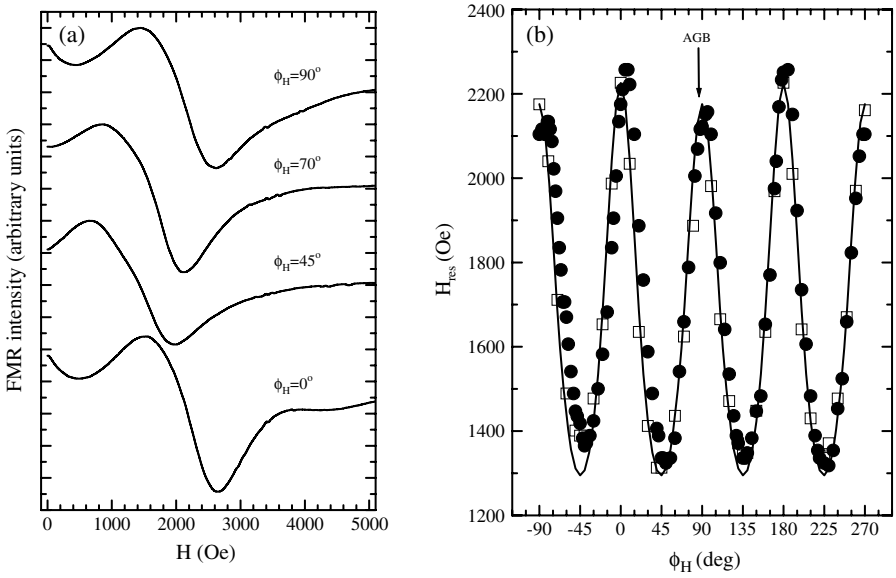

Figure 5. (a) FMR spectra for different orientations. (b) Angular variation of $H_{\rm res}$. The filled and empty circles are two sets of measured values; the solid line is the numerical calculation. $T = 125$ K.

of magnetization of the films, while the {100} directions are difficult. This observation is in good agreement with previous literature data reported on single-crystalline (La, Sr)MnO_3 grown on $SrTiO_3$ [21].

The magnetic anisotropy of the films was investigated by analysing the angular variation of $H_{\rm res}$. We have performed a systematic FMR study, recording the spectrum for different orientations of the sample and taking the value of the resonance field. The results obtained from two independent sets of measurements are shown in the right panel of figure 5. The angular variation of $H_{\rm res}$ presents a sinusoidal-like shape, where the measured values approximately span an 800 Oe amplitude range, between 1300 and 2100 Oe. A dominant fourfold symmetry with a superimposed 180° periodicity of smaller amplitude is evident. As noted above, the minima are located near the {110} directions (45° off the AGB), while the orientations parallel (90°) and perpendicular (0°) to the AGB are local maxima. However, these directions are not equivalent; the difference in height between these maxima indicates the existence of an uniaxial anisotropy whose easy axis is parallel to the AGB.

In order to quantitatively interpret the FMR results we must first consider the free energy density of each half of the bicrystalline film ($E_{\rm half}$). Let us write the different contributions as follows:

$$E_{\rm half} = E_{\rm Zeeman} + E_{\rm shape} + E_{\rm anisotropy} \tag{2}$$

where $E_{\rm Zeeman} = -\mathbf{H}\cdot\mathbf{M} = -MH\cos(\phi - \phi_H)$, M being the magnitude of the macroscopic magnetization vector. The shape term can be written as

$$E_{\rm shape} = (2\pi M^2 + K_n)\cos^2\theta \tag{3}$$

where the $2\pi M^2$ term is the usual expression that accounts for the demagnetizing energy of a thin slab. The K_n term has been added to account for an extra contribution to the 'out-of-plane' uniaxial anisotropy that could arise from substrate effects.

As $E_{\rm anisotropy}$ in (2) should account for the symmetries observed in the angular variation of $H_{\rm res}$, we must include both the uniaxial and cubic anisotropy contributions:

$$E_{\rm uniaxial} = K_u[1 - \cos^2(\phi - \phi_{\rm u})\sin^2\theta] \tag{4}$$

$$\begin{aligned} E_{\rm cubic} = {} & K_4 \sin^2\theta \sin^2\phi(\sin^2\theta\cos^2\phi + \cos^2\theta) \\ & + (\sin^2\theta\cos^2\phi\cos^2\alpha + \cos^2\theta\sin^2\alpha \\ & + \tfrac{1}{2}\sin 2\theta \sin 2\alpha\cos\phi)(\sin^2\theta\cos^2\phi\sin^2\alpha \\ & + \cos^2\theta\cos^2\alpha - \tfrac{1}{2}\sin 2\theta\sin 2\alpha\cos\phi) \end{aligned} \tag{5}$$

where α is the bicrystal angle that, depending on the half being considered, is $\pm 12°$; θ and ϕ are the magnetization angles shown in figure 2, and $\phi_{\rm u}$ is the angle that orients the uniaxial anisotropy axis, which in this case coincides with the AGB ($\phi_{\rm u} = 90°$). K_u and K_4 are the uniaxial and cubic anisotropy constants, respectively. For writing down explicitly the mathematical form of the cubic term, we have made the assumption, supported by experimental evidence from x-ray diffraction, that the three pseudo-cubic axes of the manganite film are oriented in the same way as the crystallographic axes of the substrate (see the previous section). In this context, a positive K_4 will give easy axes along the {100} directions, while a negative K_4 will give easy axes parallel (or almost parallel) to the {110} cubic directions.

From independent magnetization measurements (see the previous section) we observe that the values of the resonance field are such that the magnetization is saturated when the system attains resonance, i.e. that it is possible to define one macroscopic magnetization vector of a given magnitude on each side of the boundary, and whose spatial orientation will be given by the balance between the anisotropy, Zeeman and shape energies at each side. Note, however, that the cubic term (5), which is the only one that actually depends on α,

is quadratic in α. This means that the magnetocrystalline cubic energy density, and therefore the total energy density, has exactly the same expression for each half of the bicrystal. This means that both halves of the sample will tend to align their corresponding magnetization vectors according to the same minima of the energy density. Assuming values for the saturation magnetization and the anisotropy constants compatible with previous results found in (La, Sr)MnO_3 films [30] we observe that the Zeeman term dominates and therefore the energy density has only one minimum, close to the external field direction. Therefore, the FMR spectrum will consist of two coinciding resonance lines, as supported by our experimental findings. This assumption can be accepted with reasonable safety by recalling the x-ray diffraction results from the bicrystalline substrate and the mathematical expression of the cubic anisotropy energy given above. This fact warns about the important role that an appropriate structural characterization of the bicrystals plays in the problem. In what follows we will concentrate on the hypothesis of a single FMR line.

Magnetic resonance frequency (ω_{res}) is a direct measure of the free energy density at the equilibrium point (ϕ_{eq}, θ_{eq}) of the macroscopic magnetization vector. The Smith–Beljers (SB) equation (6) gives the relation between ω_{res} and the second derivatives of the energy density, when a ferromagnetic system is at resonance [31]. It is

$$\left(\frac{\omega_{res}}{\gamma}\right)^2 = \frac{1}{M_{sat}^2 \sin^2\theta}[E_{\theta\theta}E_{\phi\phi} - (E_{\theta\phi})^2] \qquad (6)$$

where γ is the gyromagnetic ratio and

$$E_{\theta\theta} = \frac{\partial^2 E}{\partial\theta^2}(\phi_{eq}, \theta_{eq}), \qquad E_{\phi\phi} = \frac{\partial^2 E}{\partial\phi^2}(\phi_{eq}, \theta_{eq}),$$
$$E_{\theta\phi} = \frac{\partial^2 E}{\partial\theta\partial\phi}(\phi_{eq}, \theta_{eq}). \qquad (7)$$

In an FMR experiment, the working microwave frequency is fixed, while the static magnetic field is continuously swept. Therefore, the left-hand side of (6) is a constant. For given M, the value of H_{res} for each set of parameters (K_u, K_n, K_4) is obtained by solving (6) and (7) in a self-consistent way by minimizing the energy density. The collection of consecutive iterations of this process for each orientation of the sample constitutes a simulation of the angular variation $H_{res}(\phi_H)$. By comparing the simulation with the experimental data, and varying (K_u, K_n, K_4) appropriately, we found the optimum set of values for the anisotropy constants. Taking a value of $M = 380$ emu cm^{-3} obtained from magnetization measurements, we verified that an energy density given by the expressions (2), (4) and (5) nicely reproduces the experimental angular variation of H_{res} if we set

$$K_4 = (-1.05 \pm 0.03) \times 10^5 \text{ erg cm}^{-3}$$
$$K_u = (1.52 \pm 0.20) \times 10^4 \text{ erg cm}^{-3} \qquad (8)$$
$$K_n = (6.2 \pm 0.40) \times 10^4 \text{ erg cm}^{-3}.$$

The magnetocrystalline anisotropy constant is in good agreement with previously reported data, obtained in epitaxial thin films of similar (La, Sr)MnO_3 composition [23, 27, 38]. A uniaxial anisotropy of the same magnitude has been generally measured in (La, Sr)MnO_3 films grown on $SrTiO_3$ [23, 27]. The perpendicular anisotropy constant, K_n, is comparable with values measured in other (La, Sr)MnO_3 films, like $La_{0.6}Sr_{0.4}MnO_3$ [25].

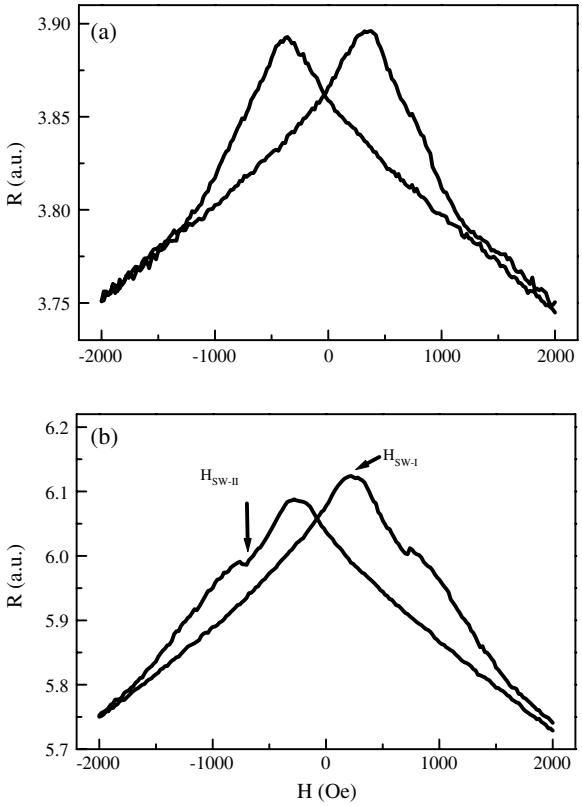

Figure 6. Magnetoresistance curves for the (a) SC and the (b) AGB arms, measured at 77 K.

5. Transport measurements

The magnetoresistance has been measured in two regions of the bicrystalline film by means of the lithographed Wheatstone bridge. The SC arm traverses the single-crystalline region of the sample while the two AGB arms are the ones that cross the artificial grain boundary. In figure 1 the corresponding measured voltages (V_{SC} and V_{GB}) are indicated. Typical magnetoresistance curves obtained for these two cases are shown in figure 6. All the transport results shown in this section were obtained at $T = 77$ K.

The resistance in both cases decreases with increasing magnetic field and is hysteretic at low field. Moreover, the magnetoresistance curves are strongly dependent on the magnetic field direction. To get a deeper insight into this aspect and to contribute to the comprehension of the low-field magnetoresistive effect in manganites, we have studied the dependence of the magnetoresistance curves and resistance on the angle ϕ_H (see section 2). The field was rotated in the plane of the films, from $0° \leqslant \phi_H \leqslant 360°$, while the current direction was kept constant.

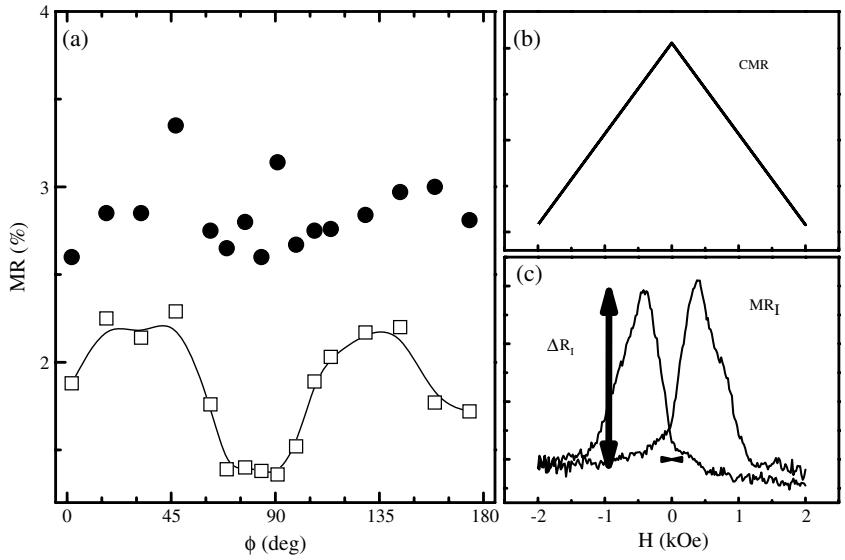

Figure 7. Angular (a) and field ((b) and (c)) dependence of the magnetoresistance components at the SC arm, measured at $T = 77$ K. (●) CMR; (□) MR$_I$.

Due to the zig-zag geometry of the circuit, the resistance measured in each branch, R, is given by

$$R = R_x + R_y \tag{9}$$

where R_y is the resistance of the paths where the electrical current flows parallel to the AGB, while R_x corresponds to the paths where the current is perpendicular to the AGB. The length/width ratio of the R_x paths is six times larger than that of the R_y ones. For this reason, the measured value is approximately equal to R_x.

The magnetoresistance curves measured at the single-crystalline (SC) region (figure 6(a)) can be described by a sum of two contributions, a high-and a low-field component as shown in the right panel of figure 7. The high-field component varies linearly with the magnetic field and is reversible. This contribution is associated with the colossal magnetoresistance (CMR) effect [1, 32] observed in ferromagnetic manganites. These compounds have a ferromagnetic to paramagnetic transition together with a metal–insulator (MI) transition that occurs close to the Curie temperature. A huge drop of resistivity as a function of magnetic field is observed around the magnetic ordering temperature, as a consequence of the MI transition. For this reason, the CMR peaks around T_{MI}. The angular dependence of the CMR ratio, defined as CMR $= (R(H = 0) - R(H = 2\ \mathrm{kOe}))/R(H = 0) * 100$, is shown in figure 7 (a). No appreciable change of the CMR with ϕ_H is observed, within the experimental scatter of the data.

The low-field magnetoresistance ratio is calculated as $\mathrm{MR}_I = \Delta R_I/R(H = 0\ \mathrm{Oe}) * 100$. ΔR_I is estimated after subtracting the CMR background component[3], see figure 7(c). MR$_I$ does depend on ϕ_H, with a fourfold symmetry plus a uniaxial anisotropy along the y axis (AGB direction). The MR anisotropy is quite similar to that of the magnetic anisotropy of the LSMO thin film.

[3] The CMR component is extrapolated assuming a linear dependence of $R(H)$ from the high fields to zero.

The magnetoresistance curves determined by measuring the V_{GB} voltage across the two AGB arms exhibit a partially different aspect (figure 6(b)). A third magnetoresistive component arises from the R versus H curves which is more noticeable in a narrow window of angles, close to $\phi_H = 0°$. The MR$_{\mathrm{I}}$ term presents almost the same angular dependence as the one measured in the single-crystalline arm. The other low-field contribution, defined as $\mathrm{MR}_{\mathrm{II}} = \Delta R_{\mathrm{II}}/R(H = 0\ \mathrm{Oe}) \times 100$ (see inset in figure 8) changes strongly with the orientation of the magnetic field. The MR$_{\mathrm{II}}$ ratio is similar to the MR$_{\mathrm{I}}$ ratio and varies roughly from one to three percent in the detectable angle range. Both the MR$_{\mathrm{I}}$ and the MR$_{\mathrm{II}}$ ratios were calculated after subtracting the CMR background contribution. The colossal magnetoresistance is still present in the measurements performed across the AGB arms, but due to the field window of the measurements and the appearance of a third magnetoresistance effect commented on above, it is difficult to quantitatively estimate its ratio.

Figure 9 shows the dependence of the magnetoresistance switching fields on the angle ϕ_H. The switching fields, $H_{\mathrm{SW-I}}$ and $H_{\mathrm{SW-II}}$, were defined as the magnetic field values where the corresponding local magnetoresistance maxima are observed in the $R(H)$ curves (see figure 6). The distinction of the MR$_{\mathrm{I}}$ and the MR$_{\mathrm{II}}$ components is difficult when the maximum positions of both effects, $H_{\mathrm{SW-I}}$ and $H_{\mathrm{SW-II}}$ are very close. However, the rapid increase of $H_{\mathrm{SW-II}}$ for $-1/4\pi \leqslant \phi_H \leqslant 1/4\pi$ allows us to distinguish both phenomena. The angular dependence of the switching field at the MR$_{\mathrm{I}}$ maxima, $H_{\mathrm{SW-I}}$, is similar to that of the coercive field (see figure 4). The $H_{\mathrm{SW-II}}$, instead, increases rapidly as the magnetic field direction approaches the perpendicular to the AGB (i.e. $\phi_H = 0°$).

The $R(H)$ curves reveal the existence of more than one magnetoresistive component at the AGB. However, the difficulty to accurately uncouple the different components from the $R(H)$ curves limits the analysis. For this reason, and in

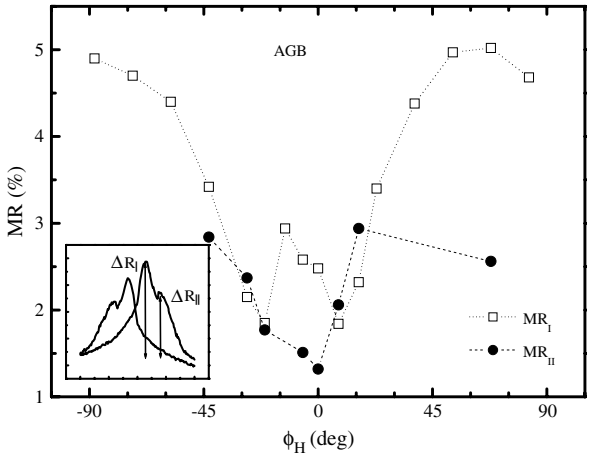

Figure 8. Angular dependence of magnetoresistance components MR_I (□) and MR_{II} (●), as measured from the V_{GB} voltage.

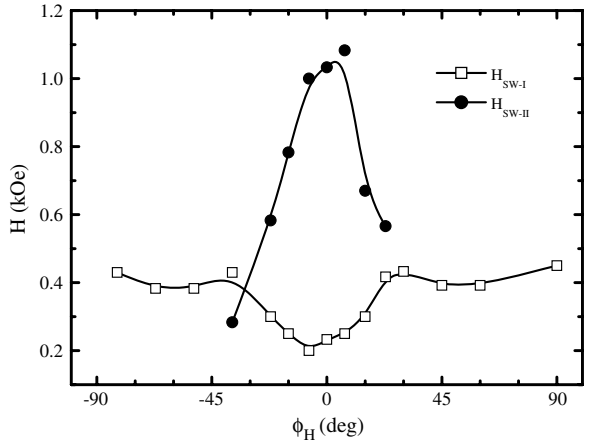

Figure 9. Switching field H_{SW} of the (□) MR_I and (●) MR_{II} components as a function of ϕ_H.

order to determine the origin of the different magnetoresistive effects, we performed complementary experiments where the angular dependence of the resistance was measured, keeping the temperature and the magnitude of the magnetic field constant.

The resistance measured at the single-crystalline arm of the Wheatstone bridge presents a twofold symmetry that does not change appreciably with magnetic field, for $H >$ 500 Oe. The resistance maxima appear in the direction perpendicular to the grain boundary, as shown in figure 10. The angular dependence of R_{SC} does not follow a $\cos^2\phi$ law at this low temperature, as expected for the anisotropic magnetoresistance observed in transition metal alloys [33] and manganites [34–36]. We note that this non-$\cos^2\phi_H$ behaviour persists even for H values much higher than the typical anisotropy fields of manganites, suggesting that the microscopic anisotropy parameters can be very different from the macroscopic ones [37], for example due to the microfabrication process. However, as the temperature is raised, the curves progressively approach this behaviour.

As discussed in a recent paper [35] the AMR effect in manganites is strongly affected by the symmetry of the crystal,

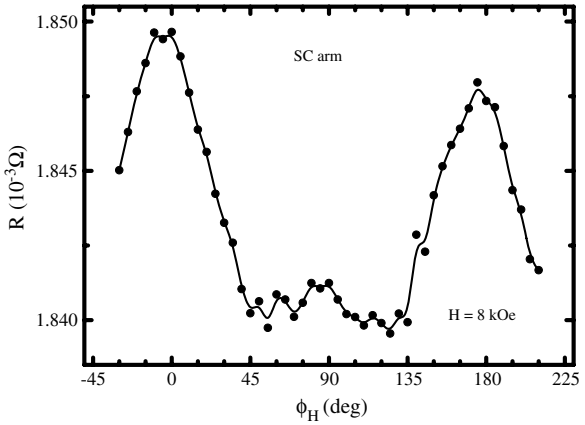

Figure 10. Angular dependence of the resistance measured on the SC arm at 77 K, and under an applied field $H = 8$ kOe.

due to the hybridization of the e_g orbitals through the spin–orbit interaction. In LSMO films grown onto (001) $SrTiO_3$ substrates, most of the authors [26, 35, 38] report that

$$\rho_{perp} > \rho_{par} \tag{10}$$

where ρ_{par} (ρ_{perp}) are the resistance values measured with the magnetic field parallel (perpendicular) to the electric current direction, respectively.

This relation depends not only on the angle between the electrical current and the magnetization, but also on the angle between the current and the manganite crystalline axes as shown by Fuhr *et al* [35] and Ziese and Sena [39]. The relation (10) is observed when the current direction is parallel to the [100] cubic axis. In our bicrystals, the ρ_{perp}/ρ_{par} ratio is inverted and this result can be explained by the fact that the electrical current is oriented 12° off the [100] axis and so the problem does not have the same orbital symmetry of previously studied samples.

The resistance measurements performed across the AGB arms present three peaks at low fields, centred at $\phi_{H,P1} = 0°$, $\phi_{H,P2} = 90°$ and $\phi_{H,P3} = 180°$. The intensity of the P1 and P3 peaks decreases strongly with increasing magnetic fields, being negligible for $H = 8$ kOe. The resistance component peaking at $\phi = 90°$, on the other hand, increases with magnetic field and saturates above 3 kOe, as seen in figure 11.

The twofold negative magnetoresistance, peaked at P1 and P3, can be explained by the existence of spin-disordered regions at the AGB. This magnetoresistance component would vanish as the magnetic field overcome the pinning induced by defects at the AGB:

$$\begin{gathered} R_{GB} + \Delta R \to R_{GB} \\ H \to \infty. \end{gathered} \tag{11}$$

The appearance of this effect has been suggested by Schiffer and co-workers in [40] but has been only clearly differentiated from the other magnetoresistive components in the present work.

Instead, the maximum of resistance observed for $\phi_H = 90°$, i.e. the electrical current perpendicular to

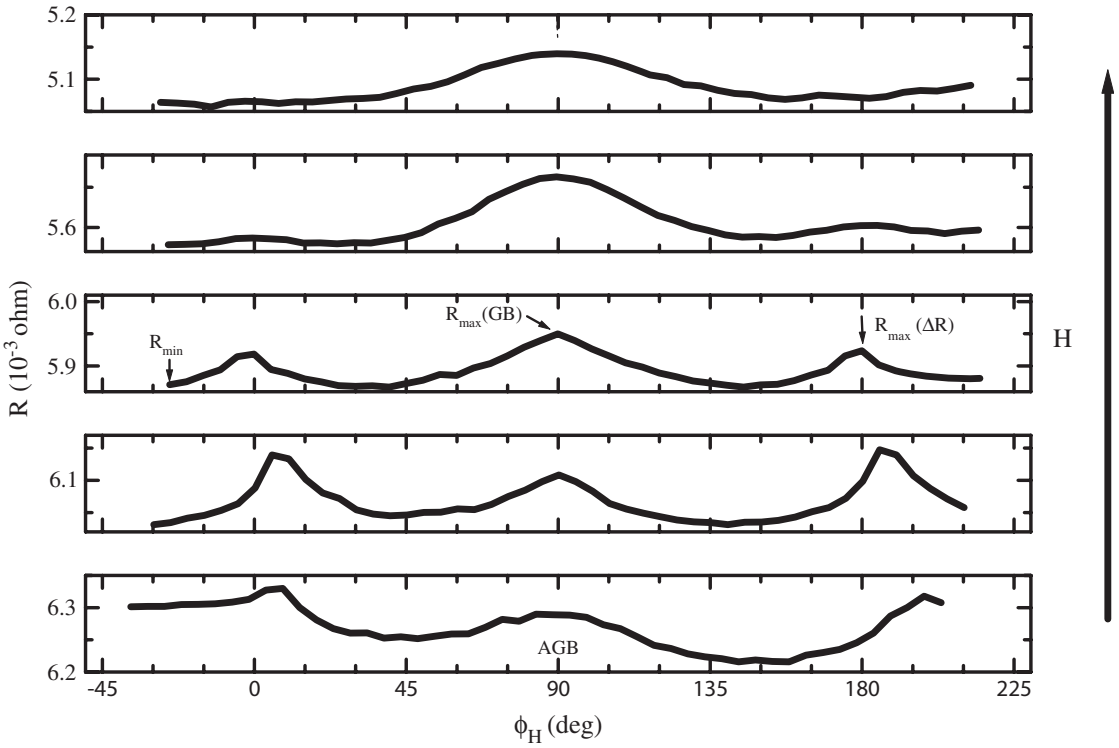

Figure 11. Angular dependence of the resistance, as measured from the V_{GB} voltage at 77 K. The curves have been measured at different magnetic fields, from $H = 0.5$ kOe (bottom curve) to $H = 8$ kOe (top curve).

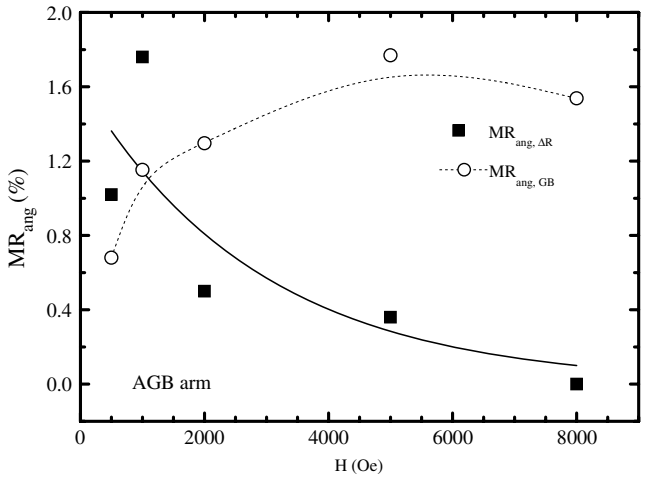

Figure 12. Field dependence of the MR_{ang} ratio, as extracted from figure 11. Calculated from R values measured at $\phi_H = 0°$ (■) and $\phi_H = 90°$ (○).

the magnetization direction, could be associated with an anisotropic magnetoresistance effect (AMR). This effect has the same symmetry as the one observed at the SC arm and therefore we assume the same physical origin. However, it is interesting to remark that the symmetry axes of both AMR effects are rotated 90°, suggesting the existence of differences in the microstructure of both regions of the sample [35, 37]. These results are summarized in figure 12, where the ratios $MR_{ang,i} = [R(\max, i) - R(\min)]/[R(\min)] \times 100$ ($i = \Delta R, GB$) calculated from the resistance versus ϕ_H curves are plotted.

$R(\min)$ varies linearly with H, scaling the high-field CMR curves mentioned above. The $MR_{ang,\Delta R}$ curve shows clearly the progressive magnetic ordering of the AGB region with the magnetic field. The $MR_{ang,GB}$, instead, saturates at $H \sim 3$ kOe. These last measurements allow us to clearly distinguish between the two low-field magnetoresistance effects observed across the AGB arms: one associated with spin disorder at the grain-boundary zone ($MR_{ang,\Delta R}$) and the other one $MR_{ang,GB}$ probably associated with the anisotropic magnetoresistance of the AGB region.

6. Conclusions

We have performed x-ray diffraction, low temperature magnetization, FMR measurements and transport experiments on bicrystalline (La, Sr)MnO_3 films. We have characterized the crystal structure and orientation, and identified and quantified the magnetic anisotropies of the unpatterned films. The angular dependence of the parameters of the magnetization hysteresis loops and the FMR spectra is consistent with a picture in which the macroscopic magnetic anisotropy consists of a (magnetocrystalline) cubic term whose axes coincide with the crystalline axes of the substrate, and a much smaller (probably stress-induced) uniaxial contribution along the AGB direction.

All the magnetoresistance curves present a colossal magnetoresistance (CMR) component that varies linearly with the magnetic field. Once the CMR has been subtracted

from the measured curves, the low-field magnetoresistance contributions were studied and characterized. The R versus H curves are hysteretic at low field and present, depending on whether they were measured on the single-crystal (SC) or on the grain-boundary (AGB) regions of the sample, one or two pairs of peaks with different physical significance. The low-field magnetoresistance measured at the SC region and one of the contributions measured across the AGB arms were associated with spin–orbit effects, i.e. the so-called anisotropic magnetoresistance (AMR). The twofold symmetry of this effect was observed in the R versus ϕ_H curves, measured at fixed magnetic field.

The other low-field component measured at the grain boundary is actually inherent to the presence of spin-disorder regions at the AGB. In fact, we have succeeded in isolating a resistive component that decreases as the magnetic field value is increased and saturates at fields higher than $H \sim 8$ kOe. This contribution is only clearly observed in a narrow ϕ_H range around the direction perpendicular to the AGB. It is worth mentioning that the peculiar crystalline orientation of our bicrystals allowed us to successfully identify a new magnetoresistive component which has arisen at the grain boundary and is associated with spin disorder.

In summary, our results indicate that the AGB structural and magnetic characteristics, which could be very complex [15], dominate and explain the low-field magnetoresistance effect.

Acknowledgments

We acknowledge Julio Pérez and Rubén Benavides for their outstanding technical support in the design and construction of the experimental set-up. We also thank Dr A Butera for the critical reading of the manuscript and Dr D García for useful discussions. The authors thank partial financial support from Fundación Antorchas, FONCyT (PICTS 03-13297 and 04-1725748), Universidad Nacional de Cuyo, and CONICET. GA, LBS, MS, BA and HP are members of CONICET. LBS is a fellow of the Guggenheim Foundation (2007).

References

[1] Jin S, Tiefel T H, McCormack M, Fastnacht R A, Ramesh R and Chen L H 1994 *Science* **264** 413–5
[2] Hwang H Y, Cheong S-W, Ong N P and Batlogg B 1996 *Phys. Rev. Lett.* **77** 2041–4
[3] Gupta A, Gong G Q, Duncombe P R, Lecoeur P, Trouillod P, Wang Y Y, Dravid V P and Sun J Z 1996 *Phys. Rev.* B **54** R15629–32
[4] Mathur N D, Burnell J, Isaac S P, Jackson T J, Teo B S, MacManus-Driscoll J L, Cohen L F, Evetts J E and Blamire M G 1997 *Nature* **387** 266–7
[5] Paranjape M, Mitra J, Raychaudjuri A K, Todd N K, Mathur N D and Blamire M G 2003 *Phys. Rev.* B **68** 144409
[6] Todd N K, Mathur N D, Isaac S P, Evetts J E and Blamire M G 1999 *J. Appl. Phys.* **85** 7263–6
[7] Philipp J B, Höfener C, Thienhaus S, Klein J, Alff L and Gross R 2000 *Phys. Rev.* B **62** R9248–51
[8] Westerburg W, Martin F, Friedrich S, Maier M and Jakob G 1999 *J. Appl. Phys.* **86** 2173–7
[9] Gross R *et al* 2000 *J. Magn. Magn. Mater.* **211** 150–9
[10] Steenbeck K, Eick T, Kirsch K, Schmidt H G and Steinbeiß E 1998 *Appl. Phys. Lett.* **73** 2506–8
[11] Isaac S P, Mathur N D, Evetts J E and Blamire M G 1998 *Appl. Phys. Lett.* **72** 2038–40
[12] Gunnarsson R, Ivanov Z G, Dubourdieu C and Roussel H 2004 *Phys. Rev.* B **69** 054413
[13] Yin H Q, Zhou J S, Dass R, Zhou J P, McDevitt J T and Goodenough J B 2000 *J. Appl. Phys.* **87** 6761–3
[14] Soh Y, Evans P G, Cai Z, Lai B, Kim C Y, Aeppli G, Mathur N D, Blamire M G and Isaacs E D 2002 *J. Appl. Phys.* **91** 7742–4
[15] Soh Y, Aeppli G, Kim C Y, Mathur N D and Blamire M G 2003 *J. Appl. Phys.* **93** 8322–4
[16] Todd N K, Mathur N D and Blamire M G 2001 *J. Appl. Phys.* **89** 6970–2
[17] Ruotolo A, Oropallo A, Miletto Granozio F, Pepe G P, Perna P, Scotti di Uccio U and Pullini D 2007 *Appl. Phys. Lett.* **91** 132502
[18] Gunnarsson R, Kadigrobov A and Ivanov Z 2002 *Phys. Rev.* B **66** 024404
[19] García D J and Alascio B 2002 *Physica* B **320** 7–12
[20] Gunnarsson R and Hanson M 2006 *Phys. Rev.* B **73** 014435
[21] Lecoeur P, Trouillod P L, Xiao G, Gupta A, Gong G Q and Li X W 1997 *J. Appl. Phys.* **82** 3934–9
[22] Sirena M, Haberkorn N, Granada M, Steren L B and Guimpel J 2003 *J. Appl. Phys.* **93** 7244
[23] Granada M, Rojas Sánchez J C, Steren L B and Leyva G 2006 *Physica* B **384** 68–70
[24] Rojas Sánchez J C, Granada M, Steren L B, Mazzaro I and Mosca D H 2007 *Appl. Surf. Sci.* **254** 219–21
[25] Steren L B, Sirena M and Guimpel J 2000 *J. Appl. Phys.* **87** 6755
[26] Infante I C, Hrabovský D, Laukhin V, Sánchez F and Fontcuberta J 2006 *J. Appl. Phys.* **99** 08C503
[27] Wang Z H, Cristini G and Habermeier H-U 2003 *Appl. Phys. Lett.* **82** 3731
[28] Causa M T *et al* 1998 *Phys. Rev.* B **58** 3233–9
Tovar M, Alejandro G, Butera A, Caneiro A, Causa M T, Prado F and Sánchez R D 1999 *Phys. Rev.* B **60** 10199–205
[29] Alejandro G, Passeggi M C G, Ramos C A, Vega D, Causa M T, Tovar M and Senis R 2003 *Phys. Rev.* B **68** 214429
[30] Steenbeck K and Hiergeist R 1999 *Appl. Phys. Lett.* **75** 1778–80
[31] Smith J and Beljers H 1955 *Phil. Res. Rep.* **10** 113
[32] von Helmholt R, Wecker J, Holzapfel B, Schultz L and Samwer K 1993 *Phys. Rev. Lett.* **71** 2331–3
[33] Campbell I A and Fert A 1982 *Ferromagnetic Materials* vol 3 (Amsterdam: North-Holland) p 751
[34] O'Donnell J, Eckstein J N and Rzchowski M S 2000 *Appl. Phys. Lett.* **76** 218
[35] Fuhr J, Granada M, Steren L B and Alascio B 2010 *J. Phys.: Condens. Matter* **22** 146001
[36] Yau J B, Hong X, Posadas A, Ahn C H, Gao W, Altman E, Bason Y, Klein L, Sidorov M and Krivokapic Z 2007 *J. Appl. Phys.* **102** 103901
[37] Pallecchi I, Gadaleta A, Pellegrino L, Gazzadi G C, Bellingeri E, Siri A S and Marré D 2007 *Phys. Rev.* B **76** 174401–11
[38] Bason Y, Hoffman J, Ahn C H and Klein L 2009 *Phys. Rev.* B **79** 92406
[39] Ziese M and Sena S P 1998 *J. Phys.: Condens. Matter* **10** 2727–37
[40] Schiffer P, Ramirez A P, Bao W and Cheong S W 1995 *Phys. Rev. Lett.* **75** 3336–9